

# DISLOCATION GENERATION IN Si: A THERMO-MECHANICAL MODEL BASED ON MEASURABLE PARAMETERS\*

Bhushan Sopori,<sup>1</sup> Przemyslaw Rupnowski,<sup>1</sup> Davor Balzar,<sup>2</sup> and Pete Sheldon<sup>1</sup>

<sup>1</sup>National Renewable Energy Laboratory, Golden, CO 80401

<sup>2</sup> University of Denver, Denver, CO 80208

## ABSTRACT

A thermo-mechanical model for predicting dislocation distribution generated by thermal stresses in Si is described. We use an experimentally determined dislocation distribution in response to a predetermined flux to establish “initial” density. The basic thermal model and the procedure for determining this parameter are described. This approach can be applied to crystal growth and other cell fabrication steps to establish thermal conditions that can minimize dislocation generation for improved solar cell performance.

## INTRODUCTION

Dislocations have a very strong influence on the performance of a Si solar cell. A major reason for this is that dislocations interact with impurities, causing impurity segregation at the dislocation sites. Impurity precipitation can also occur in the regions of high dislocation densities (also called defect clusters). Because precipitated impurities cannot be removed by the conventional gettering techniques, dislocation clusters can cause severe degradation of the cell performance. Indeed, it is now known that dislocation clusters are the primary factors limiting the performance of current commercial mc-Si solar cells [1].

Although dislocations in Si can be generated in any high-temperature processing step, the dislocations in photovoltaic silicon (PV-Si) are primarily generated during crystal growth [2]. High-speed growth generates excessive thermal stresses with concomitant high-density intragrain defects such as dislocations. Current mc-Si wafers and ribbons have dislocation densities in the range of  $10^5$  to  $10^6/\text{cm}^2$  and typical efficiencies of 14%–15%. To reach efficiencies of 18% or higher, dislocation density must be lowered below  $10^5/\text{cm}^2$ . Carefully developed thermal profiles during crystal growth are needed to achieve low dislocation densities. Unfortunately, the current thermal models cannot adequately handle dislocation generation in PV-Si. Hence, targeted studies are needed to address the dislocation reduction in PV-Si, particularly for mc-Si.

## LIMITATIONS OF PREVIOUS THERMAL MODELS

Considerable work has been done to develop thermal models for predicting elastic and plastic stresses, buckling,

and residual stresses during crystal growth. However, very little work has been done to relate the thermal profiles to dislocation generation. Much of the work by previous authors uses the concept of dislocation multiplication as the mechanism of dislocation propagation, which requires the presence of existing dislocations, often referred to as the “initial” dislocation density [3–7]. To date, the value of this parameter has been arbitrarily adjusted to match theory with experiment. Using this concept, Dillon, Sumino, and Hassen (DSH) established a commonly used relationship between dislocation generation and stress/strain relationship. Unfortunately, little or no data exist on the experimental verification.

According to this model, the total strain rate,  $\dot{\epsilon}_{ij}$ , is given by

$$\dot{\epsilon}_{ij} = \frac{1-\nu}{E} \dot{\sigma}_{ij} - \frac{\nu}{E} \dot{\sigma}_{kk} \delta_{ij} + \alpha \dot{T} \delta_{ij} + \dot{\epsilon}_{ij}^{pl}, \quad (1)$$

the plastic strain rate,  $\dot{\epsilon}_{ij}^{pl}$ , is

$$\dot{\epsilon}_{ij}^{pl} = \frac{bk_0 N_m e^{-Q/kT} (\sqrt{J_2} - D\sqrt{N_m})^p}{\sqrt{J_2}} S_{ij}, \quad (2)$$

where  $S_{ij} = \sigma_{ij} - \sigma_{kk} \delta_{ij} / 3$ ,  $J_2 = S_{ij} S_{ij} / 3$ , and

the dislocation density rate,  $\dot{N}_m$ , can be described by

$$\dot{N}_m = Kk_0 N_m e^{-Q/kT} (\sqrt{J_2} - D\sqrt{N_m})^{p+\lambda}. \quad (3)$$

In the above set of equations, Eq. 3 expresses a dislocation multiplication mechanism that involves  $N_m(0)$ , the initial dislocation density. Unfortunately, the nature of initial density is quite complex because it lumps together nucleation and the early phase of dislocation formation. It represents the behavior of the material that would contain dislocations with a density corresponding to this value. In most cases,  $N_m(0)$  is not known but its value is adjusted to give a best fit between theory and experimental results. This is one limitation of current models. Another is that the models do not include the multicrystalline nature of the wafers such as cast and ribbon mc-Si.

Because of space limitations, we will address only dislocation generation in a single-crystal material. We will use a revised concept of initial dislocation density, which includes both the nucleation phase and the initial formation of dislocations. Hence, the initial dislocation

\*This work has been authored by an employee or employees of the Midwest Research Institute under Contract No. DE-AC36-99GO10337 with the U.S. Department of Energy. The United States Government retains and the publisher, by accepting the article for publication, acknowledges that the United States Government retains a non-exclusive, paid-up, irrevocable, worldwide license to publish or reproduce the published form of this work, or allow others to do so, for United States Government purposes.

density depends on a variety of factors, which are characteristics of the material and the crystal growth process (such as nucleation sites, impurities, presence of microdefects). To accomplish this, we experimentally determine “dislocation distribution” in response to a known stress and time. This approach corresponds to the material response to a known stress—a concept that is commonly used in the network analysis as an impulse response.

We have also developed a theoretical, finite-element model, similar to the DSH model, which uses experimentally determined dislocation distribution, generated in response to a known thermal stress as the input data. This approach obviates the need for initial dislocation density and is applicable even if material is dislocation free. The proposed approach will help to establish an accurate and reliable relationship between the thermal stresses and resultant dislocation distributions for single- and mc-Si wafers.

### EXPERIMENTAL APPROACH

Experimentally, we illuminate a sample (of the material to be studied) with a known optical flux and with a sharp Gaussian-like profile. We determine dislocation distribution generated in response to this incident flux. This processing is done in an optical processing furnace equipped with a linear light source (see Fig. 1), where the flux distribution can be controlled. After thermal processing, the wafers are defect-etched using the Sopori etch and examined using an optical microscope and a commercial GT-PVSCAN laser scanner to quantitatively determine dislocation distributions [8 - 10].

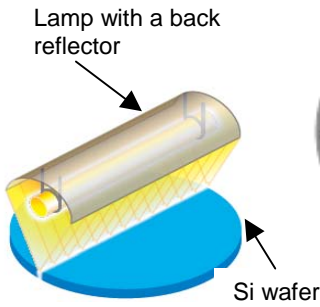


Fig. 1. Wafer processing using a linear infrared heater.

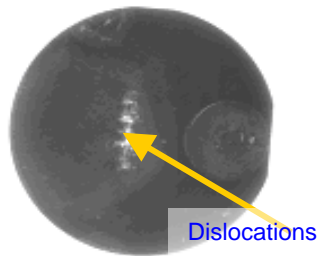


Fig. 2. A photograph of a wafer with dislocations generated.

In this paper, we will demonstrate that once the initial dislocation distribution is obtained on a given material, it can be used to identify  $N_m(0)$ , which can be used in our calculations to predict distributions corresponding to other flux profiles. Dislocations were generated in single-crystal wafers of different orientations. Figure 2 is a photograph of a 3-in wafer showing the localized region of dislocation generation. Figure 3 shows a dislocation map of a (100) sample

produced by illuminating the wafer with a static flux. The dislocation map was generated by a GT-PVSCAN. Based on these results, the maximum density of dislocations was found to equal about  $4 \times 10^6/\text{cm}^2$ . This figure also contains photographs of etch pits, showing the directions of dislocation propagation along the slip directions. One can also see a dislocation network formation caused by slip on different (111) planes. It is important to mention that dislocation generation exhibits strong dependence on the wafer orientation. For example, (111) wafers of the same size, resistivity, and surface conditions as (100) wafers, do not show evidence of dislocation generation when illuminated by the same flux profile.

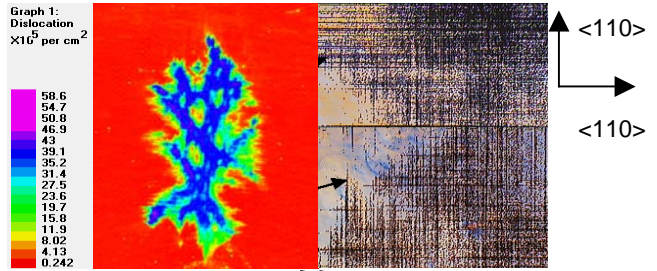


Fig. 3. Dislocation density map (a) and optical microscope images (b) of a (100) wafer after thermal processing.

To relate the generated dislocation distribution to  $N_m(0)$ , a complete thermal model must be developed, which requires the optical flux distribution. An accurate determination of the actual flux profile in an optical or RTP furnace is difficult. One of the common ways to determine the flux distribution is to analyze the optical configuration of the lamp. However, this does not yield accurate data. Our approach for obtaining such information is to determine temperature distributions in several modes and use them to fit theoretical calculations. A convenient way is to determine

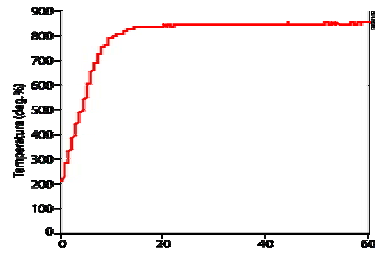


Fig. 4. Static temperature rise of a 1-in x 1-in test wafer.

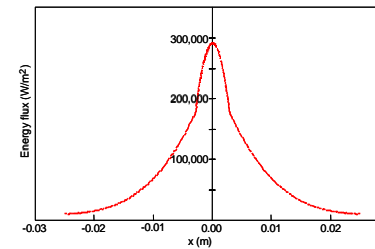


Fig. 5. Calculated flux to achieve the temperature of the test wafer rise in Fig. 4.

temperature rise at a given point on the wafer as a result of the incident flux and then use thermal modeling to arrive at a flux distribution. Figure 4 shows a measured temperature rise at the center of a 1-in x 1-in wafer. We can calculate the flux amplitude of a Gaussian-like profile required to produce this temperature rise. The calculated flux profile is shown in Fig. 5.

We can also verify the correctness of the flux profile by determining the temperature-time variation of the center of the wafer if the wafer is moved through this profile at a constant speed. Figure 6 shows a temperature Vs time profile of a 1-in x 1-in wafer as it moves through the flux profile at speed of 5 and 10 inches per minute (ipm). Next section will show the simulation results for the corresponding experimental data.

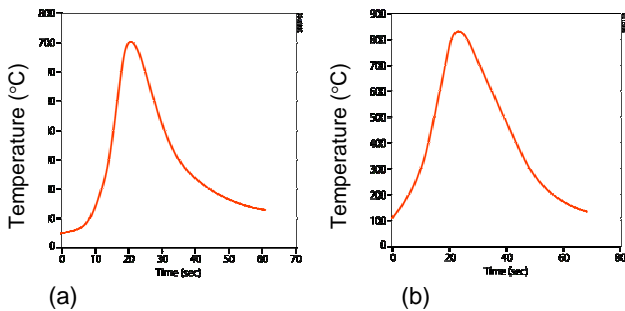


Fig. 6. Dynamic temperature profiles produced in a 1-in x 1-in wafer attached with a thermocouple. The wafer was fed at a speed of (a) 5 ipm (a) and (b) 10 ipm.

**NUMERICAL APPROACH**

Both thermal and mechanical simulations were conducted to examine the behavior of the wafer illuminated by the optical flux. In both cases, a 3-dimensional FE model of a silicon wafer was employed. These simulations were conducted using CalculiX open-source FE code (version 1.3). This code was extended to include both elasto-plastic and DSH models of Si. Calculations were performed to predict the distribution of temperature, stress, plastic strain, and dislocation

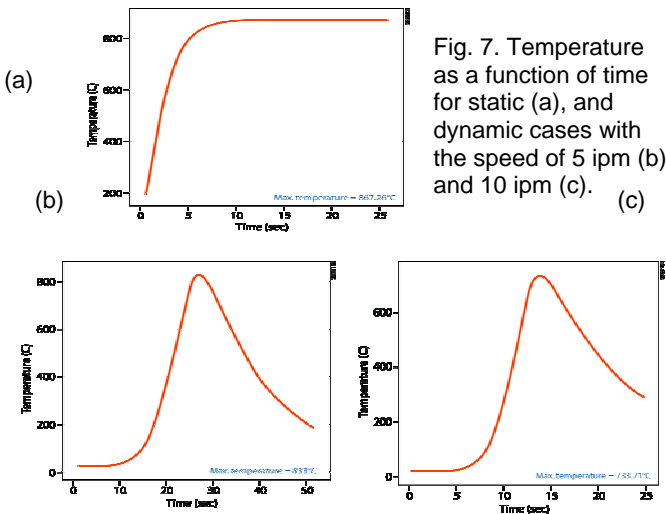


Fig. 7. Temperature as a function of time for static (a), and dynamic cases with the speed of 5 ipm (b) and 10 ipm (c).

density in circular and square wafers subjected to static heat flux of a given intensity.

Knowing the temperature rise in the middle of the test wafer (in this case 1-in x 1-in) and the distribution function of the flux (geometry of the lamp), this model can be used to build a flux profile. The flux profile synthesized to give the temperature profile of Fig. 4 is shown in Fig. 5. It is important to further verify if the flux profile is consistent with other experimental observations. This can be verified by calculating temperature rise and dynamic profiles corresponding to Figs. 4 and 6. These calculated temperature profiles are shown in Fig. 7. Figure 7a is the calculated static temp-time profile corresponding to measured profile of Fig. 4. Figures 7b and 7c show the calculated dynamic profiles corresponding to measured profiles of Fig. 6. It can be seen that there is an excellent agreement between the measured and calculated profiles. One can also see the effect of speed on the dynamic temperature profile. It is seen that the highest temperature reached by the thermocouple attached to the Si wafer is 833 °C at 5 ipm and 733 °C for 10 ipm. Both temperatures are lower than the static case of 867 °C. These temperatures are in good agreement with the measured temperature profiles. It is also seen that temperature profiles are asymmetric.

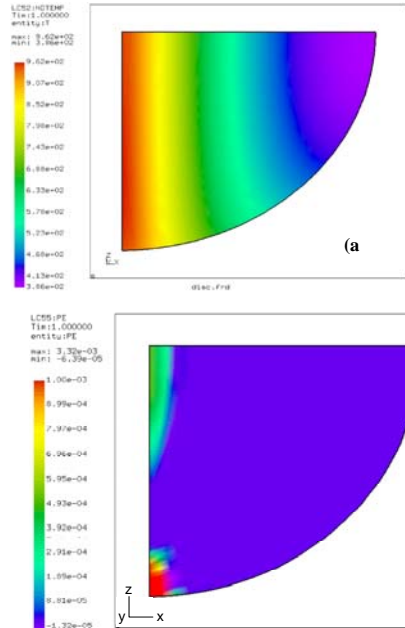


Fig. 8. Numerically predicted distribution of (a) temperature, (b) distribution of plastic strain, and (c) digital image of a (100) wafer after thermal processing.

Figures 8a and 8b depict the results of the numerical computations from both thermal and mechanical models. Figure 8a shows calculated temperature distribution of the wafer (because of the symmetry, only lower right quadrant of the wafer is shown). It is seen that very high temperature gradients exist between the center (962°C) and the cold edge (386°C) of the wafer. Note that the temperature distribution observed in Fig. 8a was generated by only one linear heater that focuses energy along the line going through the center of the wafer ( $x=0$ ). We calculated the stress distribution for the temperature profile of Fig. 5 for purely elastic and elasto-plastic regimes. Figure 8b shows the distribution of the plastic strain on the wafer surface. It is obvious that material has yielded in the regions of high stresses and high temperature. It is fruitful to compare the predicted plastic deformation of Fig. 8b with the observed dislocation distribution. Figure 8c shows actual dislocation distribution as a photograph of the defect-etched wafer after thermal treatment. One can note an excellent qualitative agreement between the two.

It may be pointed out that the best correlation between the experimentally generated dislocation density and plastic strain occurs for an initial dislocation density of  $2/\text{cm}^2$  in DSH model. Thus, our experiment actually simplifies the determination of this parameter. Now we can use this value to perform other calculations. Figure 9 depicts the time-dependent maps of the density of dislocation distributions generated by the flux distribution of Fig. 5, for several time periods up to 25 s. These distributions are in excellent agreement with measured distributions.

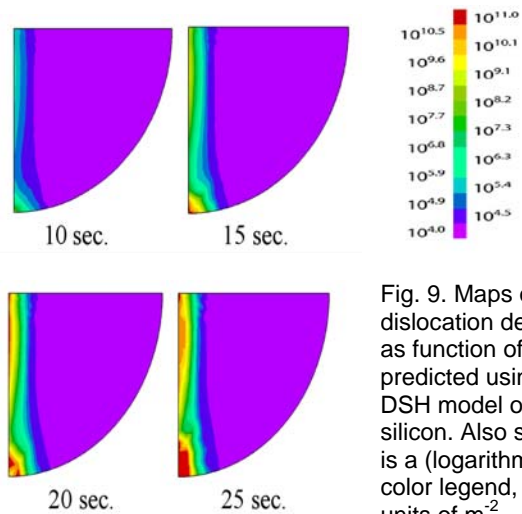


Fig. 9. Maps of dislocation density as function of time predicted using DSH model of silicon. Also shown is a (logarithmic) color legend, in the units of  $\text{m}^{-2}$ .

## CONCLUSIONS

We have verified that the results from a simple experimental approach described here can be used as an input to a theoretical model to accurately predict dislocation distributions resulting from a given temperature profile. This method obviates the need for arbitrarily fitting calculations with a dislocation

generation. We are now working with some crystal growers to apply this method to ribbons and castings for which the temperature distributions are known. We will use our experimental procedure to evaluate dislocation responses for their materials. We will compare our numerical results based on the response function with the experimental data to establish a correct and reliable thermo-mechanical model of silicon.

## REFERENCES

- [1] B.L. Sopori, C. Li, S. Narayanan, and D. Carlson, *Proc. MRS Meeting* **864**, 233 (2005).
- [2] R.W. Gurtler, "Nature of thermal stresses and potential for reduced thermal buckling of thin silicon ribbon growth at high speeds," *J. Crystal Growth* **50**, 69, 1980.
- [3] K. Sumino, Dislocations and mechanical properties of silicon, *Materials Science and Engineering* **B4**, 335, 1989.
- [4] O.W. Dillon, C.T. Tsai, and R.J. DeAngelis, "Dislocation dynamics of web type silicon ribbon," *J. Crystal Growth* **82**, 50, 1987.
- [5] D. Franke, "Numerische Simulation der Versetzungsmultiplikation in multikristallinem Silicium aus der gerichteten Blockkristallisation," Ph.D. dissertation, Aachen: Shaker, 2001.
- [6] D. Maroudas and R.A. Brown, "On the prediction of dislocation formation in semiconductor crystals grown from the melt: analysis of the Hassen model for plastic deformation dynamics," *J. Crystal Growth* **108**, 399–415, 1991.
- [7] G. Bentini, L. Corraera, and C. Donolato, "Defects induced in silicon wafers during rapid isothermal annealing: Thermoelastic and thermoplastic effects," *J. Applied Physics* **56**, 2922–2929, 1984.
- [8] B.L. Sopori, "A new defect etch for polycrystalline silicon," *J. Electrochemical Society* **131**, no. 03, pp. 667–672, 1984.
- [9] B.L. Sopori, R. Murphy, and C. Marshall, "Scanning defect-mapping system for large-area silicon substrates," *Conference Record of the IEEE Photovoltaic Specialists Conference*, 190–196, 1993.
- [10] <http://www.gtsolar.com/products/pvscan.php>.

## ACKNOWLEDGMENTS

NREL's contribution to this work was supported under Contract No. DE-AC36-99GO10337 with the U.S. Department of Energy. The authors would like to thank Jesse Appel, Thurston Melson, and Michael Speed for their help with the experiments.